Investigation of Poly(2,5)-benzimidazole (ABPBI)–Carbon Nanotube Composites for LEO Applications: An Integrated Computational and Experimental Study

Luwy Swanepoel[1], Lynndle Square[1,2], Kingsley Obodo[1,2,3], Lionel Fourie[4] and Christopher Arendse[4]

[1]Centre for Space Research, North-West University, Potchefstroom, 2531, South Africa
[2]National Institute for Theoretical and Computational Sciences, NITheCS, South Africa
[3]School of Agriculture & Science, University of KwaZulu-Natal, Scottsville, Pietermaritzburg, 3209, South Africa
[4]Department of Physics and Astronomy, University of the Western Cape, Bellville, Cape Town, 7535, South Africa

E-mail: 34200894@mynwu.ac.za

Abstract. This study investigates poly(2,5)-benzimidazole (ABPBI) enhanced with carbon nanotubes (CNT) as a potential material for space applications in Low Earth Orbit (LEO), using both computational and experimental approaches. Multi-walled carbon nanotubes (MWCNTs) were experimentally integrated into ABPBI films at 1–3 wt% via hot-casting. Powder X-ray diffraction (p-XRD), ultraviolet–visible (UV–Vis) absorption, and photoluminescence (PL) spectroscopy were used to characterise these composites. Noticeable blue shifts in the absorption maxima, widened Stokes shifts, and changes in photoluminescence with increasing MWCNT content confirmed stronger electronic coupling. Computationally, single-walled carbon nanotube (SWCNT) supercells with adsorbed ABPBI monomers were modelled and optimised using density functional theory (DFT). Simulated absorption spectra, band structures (BS), and density of states (DOS) revealed a reduced band gap and increased UV absorption due to strong π–π stacking interactions. Both methods consistently showed that CNTs tuned the optical and electronic properties of ABPBI, making it suitable for future space applications. However, further studies are recommended to explore its long-term thermal stability and mechanical durability under extended LEO exposure.

1. Introduction

Poly(2,5)-benzimidazole (ABPBI) is a high-performance polymer known for its outstanding thermal and chemical stability, low density, and high tensile strength, essential properties for space applications where both durable and lightweight materials are needed to reduce launch costs and endure the harsh conditions of Low Earth Orbit (LEO) [1, 2, 3]. The hydrogen-rich composition of ABPBI provides natural shielding against harmful secondary radiation [1], while its large band gap and stable electronic configuration help prevent unwanted electrical conduction [3].

To enhance ABPBI's overall performance, carbon nanotubes (CNTs) are incorporated as nanofillers. CNTs provide mechanical reinforcement, increased thermal conductivity, low thermal expansion, and improved charge dissipation, critical factors for stabilising polymers in extreme environments [4, 5]. Their ability to form strong π–π interactions with the polymer enhances UV absorption and charge transfer, while their structure also provides protection against atomic oxygen erosion [2, 6].

Experimentally, multi-walled carbon nanotubes (MWCNTs) are favoured because of their multiple concentric layers, which offer better mechanical strength, bonding, and dispersion within ABPBI films. This makes them more suitable for practical fabrication and hot-casting experiments [2]. In contrast, single-walled CNTs (SWCNTs) feature a simpler, single-layer atomic structure and well-defined chirality, making them computationally efficient. Their (3,3) armchair symmetry allows for accurate simulation of nanoscale effects like orbital hybridisation and charge transfer, all while maintaining low computational demands [7].

Despite differences in structural complexity, recent studies have shown that ABPBI composites reinforced with SWCNTs, double-walled CNTs (DWCNTs), or MWCNTs display similar trends in thermal and structural property enhancements [8]. Thus, a comparison between computational and experimental results is required to provide a reliable framework to evaluate ABPBI-CNT composites for long-term use in LEO, as done in the current study.

2. Methodology

2.1. Experimental Methodology

The ABPBI/MWCNT composite was synthesised using in-situ polymerisation, previously done by [1, 9, 10], a method in which nanotubes are dispersed directly into the monomer mixture and polymerised together to enhance CNT dispersion and interaction within the polymer matrix, making it ideal for insoluble or thermally unstable polymers [5]. First, 1.5 g of phosphorus pentoxide (P_2O_5) was dissolved in 10 mL of methane-sulfonic acid (MSA) at 150°C under a nitrogen atmosphere. Then 1 g of 3,4-diaminobenzoic acid (DABA) was added and stirred for 30 minutes, after which 1–3 wt% MWCNTs were introduced and the mixture heated to 200°C until it thickened. The hot mixture was cast onto a preheated glass slab using a casting machine (1 mm thickness) and cured at 200°C. The solid membrane was removed with deionized water and purified using a sodium hydroxide–ethanol–water mixture for three days, then rinsed, pressed flat, and dried. The composite was then characterised using UV-Vis absorption, PL spectroscopy, and p-XRD.

2.2. Computational Methodology

To model the interaction between ABPBI and SWCNTs, density functional theory (DFT) calculations were performed in BIOVIA Materials Studio 2020, using CASTEP (Cambridge Serial Total Energy Package) for periodic supercell simulations and DMol^3 for isolated-molecule optimisations [7, 11, 12]. DFT solves the Kohn–Sham [13] equations based on total electron density, offering accurate electronic structure predictions at a fraction of the cost of wavefunction methods [14, 15]. All jobs were executed on the NICIS CHPC (National Integrated Cyber Infrastructure System and Centre for High Performance Computing) to ensure rapid convergence [16].

The (3,3) armchair SWCNT was constructed using the nanotube builder tool. To model realistic bulk behaviour, the unit cell was extended into a supercell by repeating the structure eight times in the z-direction, thereby mimicking an infinite system while reducing interactions between periodic images of adsorbates [7, 17]. Initial parameter optimisations were performed in CASTEP to determine the most stable and computationally efficient simulation settings. By plotting the total energy against each parameter, the optimal values were determined as a 500 eV cut-off energy, a 2×2×1 k-point mesh, and lattice dimensions of 7.415×7.415×19.676 Å, corresponding to the lowest total energy configuration [10].

The ABPBI monomer was geometry optimised using the DMol^3 module with the GGA-PBE (Generalised Gradient Approximation—Perdew–Burke–Ernzerhof) functional, chosen for its balance between computational efficiency and accurate representation of the electronic structure [7, 18]. After optimisation, the monomer was positioned near the SWCNT, and the simulation box was expanded laterally to 15 Åto model isolated monomer-nanotube interactions without interference from neighbouring periodic copies.

The interaction between the optimised ABPBI monomer and the SWCNT was investigated using the Adsorption Locator module, which applies Monte Carlo algorithms to identify the most energetically favourable binding sites by sampling various orientations and positions within a defined 5 Å adsorption range [7]. Based on [10], the following procedure was executed: 18 candidate configurations were generated and manually refined by adjusting the monomer's position relative to the nanotube surface. Each configuration was evaluated using CASTEP single-point energy calculations, and the lowest-energy structure was selected. This composite system was then fully geometry-optimised in CASTEP, allowing both atomic positions and cell dimensions to relax to their lowest energy state. Key electronic properties, Density of States (DOS), Band Structure (BS), and Optical Absorption, were calculated to assess how the interaction affects conductivity, charge distribution, and optical behaviour. For accurate comparison, equivalent calculations were conducted on the isolated SWCNT supercell and the ABPBI monomer using the same simulation box, thereby maintaining consistent boundary conditions across all systems.

3. Results and Discussion

3.1. Experimental Results

The p-XRD pattern, determined with a PANalytical X'Pert Pro diffractometer using a cobalt X-ray tube, of the ABPBI/MWCNT composite in Figure 1 shows two broad peaks at approximately $2\theta = 12°$ and $32°$, indicating a semi-crystalline structure with both ordered and disordered regions [1]. The lower-angle peak reflects the interchain spacing of the ABPBI polymer backbone. In contrast, the higher-angle peak is associated with π–π stacking and structural contributions from the MWCNTs, suggesting partial alignment and integration into the polymer matrix [1, 19]. Compared to pristine ABPBI, the peak broadening and slight shifts imply that the incorporation of MWCNTs disrupts the regular polymer chain packing, introduces internal strain and reduces crystallite size [1]. The presence of additional minor peaks in the diffraction pattern may arise from experimental factors such as residual MSA or cobalt X-ray source artefacts. Overall, the p-XRD results support the formation of a well-integrated nanocomposite with a compact and reinforced structure.

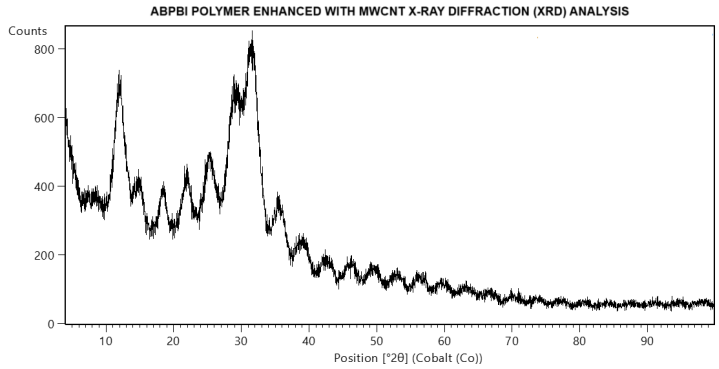

Figure 1. Experimental XRD analysis of the ABPBI-MWCNT composite

Table 1. Optical properties of ABPBI and MWCNT composites.

Composite	**Absorption**		**Emission**	
	λ_{max} (nm)	λ_{onset} (nm)	λ_{Em} (nm)	$\Delta\lambda_{St}$ (nm)
ABPBI	466	483	586	103
ABPBI/MWCNT 1 wt%	413	466	517	104
ABPBI/MWCNT 2 wt%	339	467	565	226
ABPBI/MWCNT 3 wt%	336	466	566	230

λ_{onset} = absorption peak edge; $\Delta\lambda_{St}$ = Stokes shift.

The UV-Vis absorption and PL results (Figure 2) show that pristine ABPBI strongly absorbs UV light due to π-π^* transitions along its conjugated backbone. Adding 1–3 wt% MWCNTs boosts the absorbance in the 230–450 nm region, reflecting enhanced π-π stacking and stronger interaction between the polymer and nanotubes. The absorption peak (λ_{max}) in Table 1 blue shifts from 466 nm in pristine ABPBI to 413 nm at 1 wt% and further down to 336–339 nm at higher CNT loadings, reflecting improved charge transfer and tighter electronic coupling [20, 21]. Despite these changes, the absorption edge remains stable near 466 nm (vs. 483 nm for pristine ABPBI), suggesting that the core electronic structure is preserved [22]. The emission peak shifts from 586 nm (pristine) to 517 nm (1 wt%) and slightly red-shifts to 565–566 nm at 2–3 wt%, whilst the PL intensity decreases with increased CNT content, confirming that nanotubes introduce non-radiative traps and enhance energy loss pathways [23]. The Stokes shifts, the gap between the absorption and emission peaks, became wider with CNT loading, signalling more internal energy dissipation before emission . These trends show that MWCNTs enhance UV absorption and charge transfer while suppressing emission.

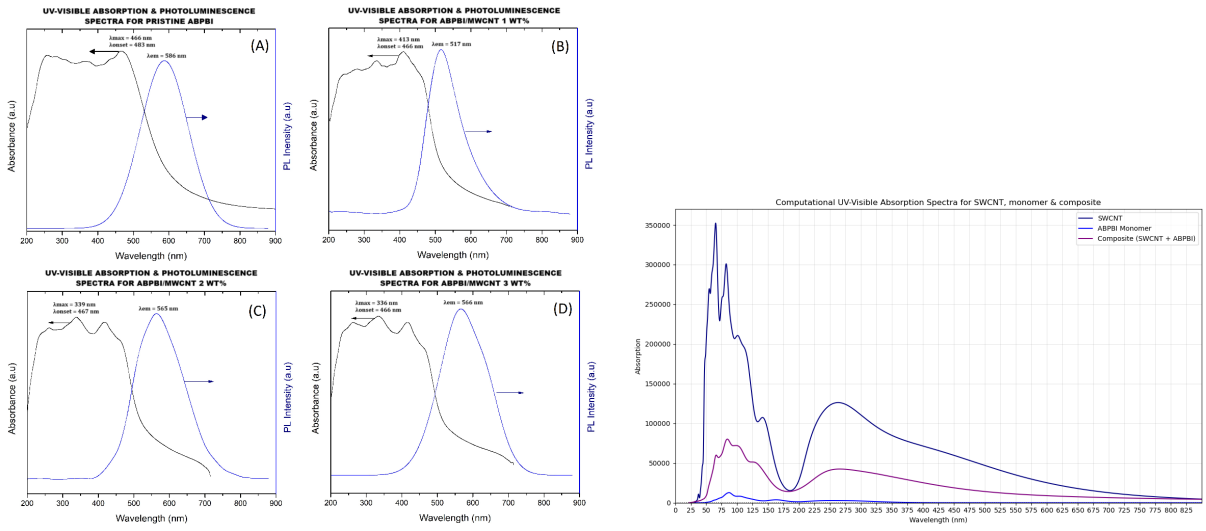

Figure 2. Left: Experimental UV–Vis and PL spectra for ABPBI/MWCNT composites; Right: Computational UV-Vis spectra for ABPBI/SWCNT composites

3.2. Computational Results

In Figure 3, the BS and DOS of the SWCNT show several bands crossing the Fermi level, confirming its metallic nature and excellent conductivity. The sharp van Hove singularities in the DOS reflect its 1D structure, meaning that electrons can only move along the nanotube axis, leading to distinct, well-defined energy levels where electrons are easily excited. These electronic features explain the strong UV absorption seen below 100 nm in Figure 2, appearing as sharp peaks caused by π–π^* transitions in the carbon–carbon double bonds.

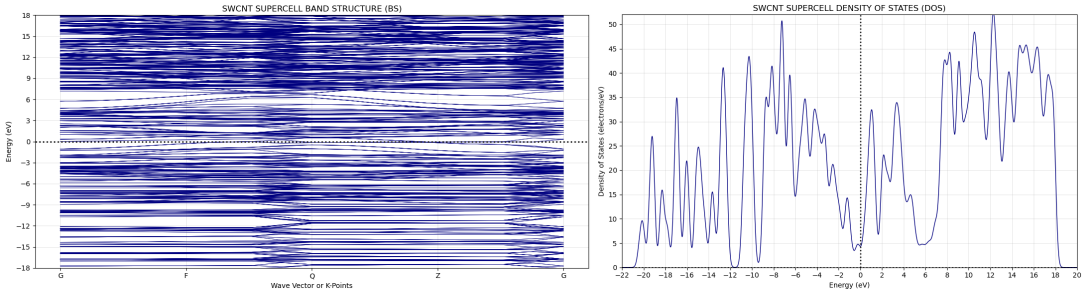

Figure 3. SWCNT simulated BS and DOS

The ABPBI monomer exhibits insulating behavior, as seen in its band structure (BS) (Figure 4), which shows a wide band gap of approximately 4.12 eV. This is supported by the density of states (DOS), which is zero at the Fermi level, indicating that electronic conduction is unlikely without significant energy input. The absorption spectrum (Figure 2) displays a strong UV peak around 100 nm, suggesting effective UV absorption due to its aromatic rings, which enable localized electronic excitations despite limited transitions due to the large band gap.

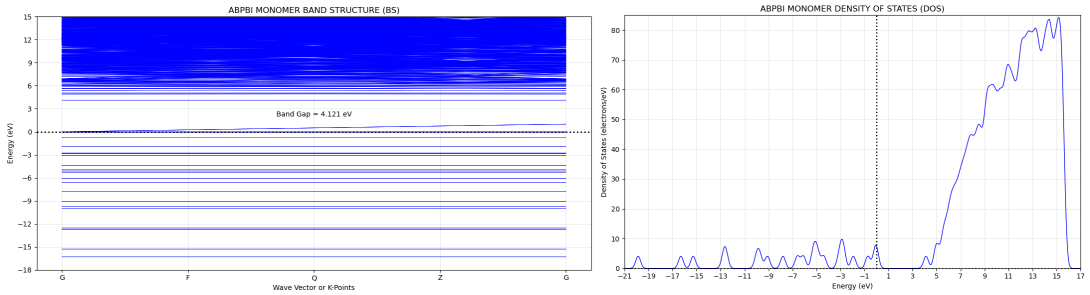

Figure 4. ABPBI monomer simulated BS and DOS

When ABPBI adsorbs onto the SWCNT surface, the BS (Figure 5) becomes denser near the Fermi level and the band gap narrows due to π–π stacking and orbital hybridization that give rise to new electronic states. The DOS shows clear peaks near 0 eV, indicating charge transfer between the polymer and nanotube. Meanwhile, the UV–vis absorption spectrum (Figure 2) maintains strong UV features but with broader and intensified peaks, reflecting improved light absorption. These changes show that adding carbon nanotubes transforms the ABPBI monomer from an insulator to a semiconductor with significantly enhanced electrical conductivity and optical performance. In contrast to the bulk ABPBI polymer, monomers exhibit larger band gaps because their highest occupied molecular orbitals (HOMO) and lowest unoccupied molecular orbitals (LUMO) are confined to a single molecule, yielding a greater energy separation.

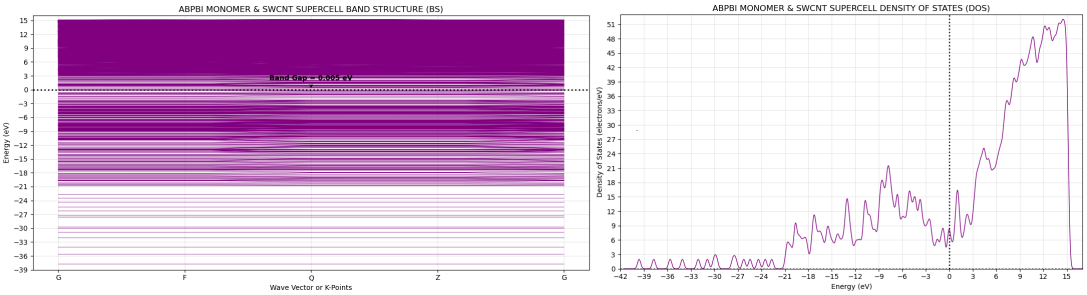

Figure 5. ABPBI-SWCNT composite simulated BS and DOS

4. Conclusion

The combined experimental and computational results demonstrate that incorporating CNTs into ABPBI significantly enhances its optical and electronic properties. p-XRD analysis shows that the addition of MWCNTs disrupts the regular packing of polymer chains, introduces internal strain, and promotes closer polymer-nanotube integration. UV–Vis spectroscopy revealed stronger UV absorption and blue shifts with increasing CNT content, indicating enhanced charge transfer and π–π interactions. PL measurements show weaker emission and larger Stokes shifts, suggesting internal energy trapping within the composite. Complementary computational studies confirm a reduced band gap and the formation of new electronic states due to π–π stacking, supporting increased conductivity and optical absorption. Together, these findings show that CNT incorporation transforms ABPBI from an insulator to a semiconductor, with computational results offering deeper insights beyond experimental reach. Overall, this highlights the strong potential of CNT–ABPBI composites for space applications.

Acknowledgements

The authors acknowledge the NRF, NASSP, North-West University Centre for Space Research, Thuthuka funding instrument (UID No. 138417) and NICIS CHPC.

References

[1] Fourie L F, Square L, Arendse C and Msimanga M 2023 *APL Materials* **11** 071103

[2] Ellis E H and Square L C 2023 *Reactive Molecular Dynamics Simulations of the Surface Interactions Between Atomic Oxygen and Poly(2,5)-Benzimidazole Carbon Nanotube Composite* Master's thesis North-West University

[3] Kittel C 1996 *Introduction to Solid State Physics* 7th ed (New York: Wiley)

[4] Yakobson B I and Avouris P 2001 *Topics in Applied Physics* **80** 287–327

[5] Fenta E W and Mebratie B A 2024 *Heliyon* **10** e36490

[6] Gutiérrez O, Prieto M, Perales-Eceiza A, Ravanbakhsh A, Basile M and Guzmán D 2023 *Electronics* **12** 4058

[7] BIOVIA, Dassault Systèmes 2023 Biovia materials studio overview `https://www.3ds.com/assets/invest/2023-10/biovia-materials-studio-overview.pdf` accessed: 2024-11-11

[8] Square L, Oryema B, Mafoko P, Ellis E and Vorster H 2025 *Radiation Physics and Chemistry* **232** 112658

[9] Square L, Fourie L F, Ellis E and Msimanga M 2023 *2023 IEEE 23rd International Conference on Nanotechnology (NANO)* 963–966

[10] Swanepoel L, Square L and Kingsley O 2024 The effect of microgravity on the abpbi carbon nanotube composite for leo applications – an experimental and computational approach unpublished Honours Report, North-West University

[11] Grillo M, Andzelm J, Govind N, Fitzgerald G and Stark K 2004 *Computational Materials Science: From Basic Principles to Material Properties* (Springer) pp 207–221

[12] de Alencar Rocha R, da Cunha W F and Ribeiro Jr L A 2019 *Journal of Molecular Modeling* **25** 290

[13] Kratzer P and Neugebauer J 2019 *Frontiers in Chemistry* **Volume 7 - 2019** ISSN 2296-2646 URL `https://www.frontiersin.org/journals/chemistry/articles/10.3389/fchem.2019.00106`

[14] Pedroza L S, da Silva A J and Capelle K 2009 *Physical Review B - Condensed Matter and Materials Physics* **79** 201106

[15] Payne M C, Teter M P, Allan D C, Arias T A and Joannopoulos J D 1992 *Reviews of Modern Physics* **64** 1045–1097

[16] CHPC 2024 About the CHPC. National Integrated Cyber Infrastructure System (NICIS) and Centre for High Performance Computing (CHPC) `https://www.chpc.ac.za/about-the-chpc/` accessed: 11 Nov. 2024

[17] Hashemi M, Sääskilahti K and Puska M J 2011 *Physical Review B—Condensed Matter and Materials Physics* **83** 115411

[18] Sarker N 2025 *EVALUATION OF COMPUTATIONAL CHEMISTRY SOFTWARE AND DENSITY FUNCTIONAL THEORY METHODS FOR ELECTRONIC STRUCTURE COMPUTATION OF PEROVSKITES* Master's thesis Itä-Suomen yliopisto

[19] Kang J Y, Eo S M, Jeon I Y, Choi Y S, Tan L S and Baek J B 2010 *Journal of Polymer Science Part A: Polymer Chemistry* **48** 1067–1078

[20] Allen C S, Liu G, Chen Y, Robertson A W, He K, Porfyrakis K, Zhang J, Briggs G A D and Warner J H 2014 *Nanoscale* **6** 572–580

[21] Davoody A, Karimi F, Arnold M and Knezevic I 2016 *The Journal of Physical Chemistry C* **120** 16354–16366

[22] Dukovic G, White B E, Zhou Z, Wang F, Jockusch S, Steigerwald M L, Heinz T F, Friesner R A, Turro N J and Brus L E 2004 *Journal of the American Chemical Society* **126** 15269–15276

[23] Habenicht B F and Prezhdo O V 2008 *Physical review letters* **100** 197402